Contribution from the Chemical Physics Program and Department of Chemistry, Washington State University, Pullman, Washington 99164-4630

# Crystal Structures and Magnetic Behavior of Two Novel Copper(II) Halide Chains. $(C_7H_{10}N)_4Cu_5Cl_{14}$ and $(C_5H_{14}N)_4Cu_5Cl_{14}$: Multiple Copper(II) Halide Coordination Geometries

Marcus R. Bond, Roger D. Willett,* and Gerald V. Rubenacker

*Received November 7, 1989*

The crystal structures of tetrakis(1,4-dimethylpyridinium) tetradecachloropentacuprate(II) ($(1,4\text{-DMP})_4Cu_5Cl_{14}$) and tetrakis(ethyltrimethylammonium) tetradecachloropentacuprate(II) ($(ETrMA)_4Cu_5Cl_{14}$) have been determined. For $(1,4\text{-DMP})_4Cu_5Cl_{14}$ the unit cell is triclinic $P\bar{1}$ with $a = 7.604$ (1) Å, $b = 9.986$ (2) Å, $c = 15.146$ (2) Å, $\alpha = 94.84$ (1)°, $\beta = 97.24$ (1)°, $\gamma = 101.61$ (1)°, and $Z = 1$. For $(ETrMA)_4Cu_5Cl_{14}$ the unit cell is monoclinic $P2_1/c$ with $a = 15.499$ (3) Å, $b = 9.063$ (2) Å, $c = 15.687$ (3) Å, $\beta = 92.56$ (2)°, and $Z = 2$. The structures refined to $R = 0.0322$ ($(1,4\text{-DMP})_4Cu_5Cl_{14}$) and $R = 0.0526$ ($(ETrMA)_4Cu_5Cl_{14}$). Both structures consist of chains of pentanuclear $Cu_5Cl_{14}^{4-}$ clusters in which the copper(II) ions occur in one of the three different coordination geometries. In $(1,4\text{-DMP})_4Cu_5Cl_{14}$ the cluster configuration is bowtie-shaped: the central copper ion (Cu(1)) of the bowtie is tetragonally distorted octahedral, the copper ions on two opposite corners (Cu(2)) are distorted square pyramidal, and the copper ions on the other two opposite corners (Cu(3)) are distorted tetrahedral. In $(ETrMA)_4Cu_5Cl_{14}$ the cluster configuration is linear: the central copper ion (Cu(1)) is in a tetragonally distorted octahedral configuration, the two copper ions (Cu(2)) on either side are 4 + 1 + 1 coordinate with a square-pyramidal distortion, and the terminal pair (Cu(3)) are distorted square pyramidal. The presence of multiple copper(II) halide geometries in these and other structures is rationalized by simple electrostatic arguments. Magnetic susceptibility data have been collected in the temperature range 2–100 K for $(1,4\text{-DMP})_4Cu_5Cl_{14}$ and 4.2–80 K for $(ETrMA)_4Cu_5Cl_{14}$. The data have been fit to a Heisenberg, spin-$^1/_2$, "bowtie" cluster model with a mean field correction to account for the intercluster interaction: $J_{13} = 0$ K, $J_{12}/k = -34.1$ (6) K, $J_{23}/k = -4.9$ (3) K, $\Theta = -7.0$ (3) K, and $g = 2.164$ (7) for $(1,4\text{-DMP})_4Cu_5Cl_{14}$; $J_{12} = J_{23} = 37.7$ (9) K, $J_{13} = 0$ K, $g = 2.05$, and $J' = -1.48$ (3) K for $(ETrMA)_4Cu_5Cl_{14}$. Fitting the region of the maximum in the $(ETrMA)_4Cu_5Cl_{14}$ susceptibility to a one-dimensional spin-$^5/_2$ Heisenberg model gives $J_{1C} \approx -10$ K. The values found for the intracluster exchange can be explained in terms of simple atomic orbital arguments. The complicated pentacoordinate geometry of the copper ions in the intercluster bridges precludes a simple orbital explanation of the intercluster exchange.

## Introduction

Copper(II) halides show a wide variety of stereochemical complexity. Observed geometries include four-coordinate species (ranging from square planar to nearly tetrahedral), five-coordinate species (spanning trigonal bipyramidal, square pyramidal, and folded or tetrahedrally distorted 4 + 1 geometries), and six-coordinate species (generally with tetragonally elongated octahedral 4 + 2 geometries).[1] This span of geometries arises not only through the inherent flexibility of the Cu(II) coordination sphere, which allows for both normal Cu–X bonds and longer, semicoordinate Cu···X bonds, but also because of the nonstereospecific nature of the rather large, spherical halide ions. The crystal chemistry of copper(II) halide salts is further complicated by the bridging ability of the halide ions. The halide ions involved in the bridge formation can either form two normal Cu–X bonds (a symmetrical bridge) or one normal Cu–X bond and one longer, semicoordinate Cu···X bond (an asymmetrical bridge). The Cu(II) ions can be bridged combinations of one, two, or three such bridges. Thus, a bewildering array of solid-state structures is possible.

Some semblance of sanity can be extracted from these structures, and a reasonable rationalization made for many of the structures, by application of simple electrostatic arguments to which we have applied the term "charge compensation". Naively, the observed stereochemistries of copper(II) halides salts can be visualized as a balance between crystal field stabilization effects (favoring square-planar, folded 4 + 1, or 4 + 2 geometries) and ligand–ligand repulsion effects (favoring a tetrahedral geometry). The square-pyramidal geometry lies between these two extremes, while the trigonal-bipyramidal geometry appears to be rather unfavorable. Thus, any factors that reduce ligand–ligand repulsions should lead to stabilization of the square-planar, folded 4 + 1, and 4 + 2 geometries, so one might anticipate these geometries to be predominant more in chloride salts than in bromide salts. More importantly, any interactions that reduce the effective charge on the halide ion should have the same effect. Thus, the presence of hydrogen bonding to the halide ions, which pulls charge from the halides, stabilizes the planar geometry. This effect has been particularly useful in understanding the thermochromic behavior of copper(II) chloride salts[2] as well as the crystal chemistry of the antiferrodistortive $A_2CuX_4$ layer perovskites.[3] Involvement of the halide ions in bridge formation will produce similar behavior, with symmetric bridge formation more effective than asymmetric bridge formation at stabilizing the planar geometry. These arguments have been used to explain much of the observed structural chemistry for $ACuCl_3$ salts.[4] The delicate balance between these various factors is most clearly seen where two (or more) of these geometries are found to occur in the same structure. In this paper, we report the structural and magnetic results of two new salts, $(1,4\text{-DMP})_4Cu_5Cl_{14}$ (1,4-DMP = 1,4-dimethylpyridinium) and $(ETrMA)_4Cu_5Cl_{14}$ (ETrMA = ethyltrimethylammonium), each of which contains copper(II) ions in three distinct coordination geometries.

## Experimental Section

**Crystal Structures. $(1,4\text{-DMP})_4Cu_5Cl_{14}$.** 1,4-Dimethylpyridinium chloride was prepared by the method for quaternization of pyridine developed by Carpio et al.[5] Copper(II) chloride was added to a 1-propanol solution of 1,4-dimethylpyridinium chloride, initially producing a yellow precipitate, which, upon further addition of copper(II) chloride, became red-brown. A portion of the washed and dried precipitate was used to grow small, single crystals of $(1,4\text{-DMP})_4Cu_5Cl_{14}$ from an ethyl acetate/nitromethane mixture by using a modified temperature-gradient technique. Large single crystals were grown by slow evaporation of a concentrated HCl solution containing stoichiometric amounts of 1,4-dimethylpyridinium chloride and copper(II) chloride. The scarlet (in color) crystals deform easily on cutting; hence, the smaller crystals were used for the structure determination.

A crystal of $(1,4\text{-DMP})_4Cu_5Cl_{14}$ was glued to a glass fiber and mounted on a Syntex $P2_1$ diffractometer upgraded to Nicolet P3 specifications (graphite monochromator). Cell constants were determined by a least-squares refinement of the angular settings of 25 well-centered reflections in the range $33° < 2\theta < 35°$.[6] Pertinent details of the data collection are listed in Table I. Data were collected in a hemisphere of

(1) Reinen, D. *Comments Inorg. Chem.* **1983**, *2*, 227–246.

(2) Bloomquist, D. R.; Willett, R. D. *Coord. Chem. Rev.* **1982**, *47*, 125–164.

(3) Willett, R.; Place, H.; Middleton, M. *J. Am. Chem. Soc.* **1988**, *110*, 8639–8650.

(4) Willett, R. D.; Geiser, U. *Croat. Chem. Acta* **1984**, *57*, 737–747.

(5) Carpio, R. A.; King, L. A.; Lindstrom, R. E.; Nardi, J. C.; Hussey, C. L. *J. Electrochem. Soc.* **1979**, *126*, 1644–1650.

(6) Campana, C. F.; Shepard, D. F.; Litchman, W. M. *Inorg. Chem.* **1981**, *20*, 4039–4044.

0020-1669/90/1329-2713$02.50/0 

**Table I.** Data Collection and Structure Refinement Conditions and Parameters for $(1,4\text{-DMP})_4Cu_5Cl_{14}$ and $(ETrMA)_4Cu_5Cl_{14}$

| | $(1,4\text{-DMP})_4Cu_5Cl_{14}$ | $(ETrMA)_4Cu_5Cl_{14}$ |
|---|---|---|
| empirical formula | $C_{28}H_{40}N_4Cu_5Cl_{14}$ | $C_{20}H_{56}N_4Cu_5Cl_{14}$ |
| MW | 1246.724 | 1166.76 |
| space group | $P\bar{1}$ | $P2_1/n$ |
| lattice consts, Å and deg | $a$ = 7.604 (1) | 15.499 (3) |
| | $b$ = 9.986 (2) | 9.063 (2) |
| | $c$ = 15.146 (2) | 15.687 (3) |
| | $\alpha$ = 94.84 (1) | 90 |
| | $\beta$ = 97.24 (1) | 92.56 (2) |
| | $\gamma$ = 101.61 (1) | 90 |
| $V$, Å$^3$ | 1110.6 (3) | 2201.5 (8) |
| radiation ($\bar{\lambda}$, Å) | Mo K$\alpha$ (0.71069) | |
| abs coeff, cm$^{-1}$ | 32.43 | 39.4 |
| $\rho_{calc}$, g cm$^3$ | 1.86 | 1.76 |
| $Z$ | 1 | 2 |
| $R$ | 0.0322 | 0.0526 |
| $R_w$[a] | 0.0447 | 0.0455 |
| function minimized[a] | $\sum w(\|F_o\| - \|F_c\|)^2$ | |

[a] $w = [\sigma^2(F) + gF^2]^{-1}$. g = 0.000 33 and 0.000 16, respectively.

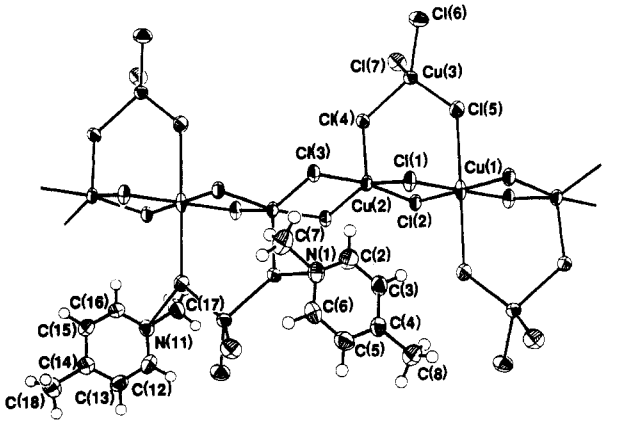


**Figure 1.** View of the chain structure and of the two crystallographically inequivalent cations in $(1,4\text{-DMP})_4Cu_5Cl_{14}$. Open bonds denote the N···Cl contact between the cations and the chain.

reciprocal space ($0 \le h \le 10, -12 \le k \le 12, -19 \le l \le 19$). Intensities of three check reflections were measured periodically (every 93 reflections) during the data collection, variations within counting statistics. Crystal decay, Lorentz–polarization, and absorption corrections were applied to the data. Crystal structure solution and refinement were achieved by using the SHELXTL package of programs.[7] A four-atom fragment, $Cu_2Cl_2$, of the structure was identified from the Patterson map, one copper atom of the fragment was placed at the origin of the unit cell, and structure refinement was initiated. Coordinates of the remaining atoms were identified from subsequent electron-density difference maps and included in the structure. Assignment of the nitrogen atom positions is ambiguous when determined by the geometry of the cation alone. Of the two possible nitrogen sites on the cation, the one with the larger peak on the electron density difference map was chosen in each case. Refinement of the nitrogen atoms in these positions gave thermal parameters comparable in magnitude to those of the other ring atoms. Besides, there are some relatively short N···Cl interactions at the chosen sites but not at the alternate sites, further justifying the choice of nitrogen atom coordinates. Anisotropic thermal parameters were refined for all nonhydrogen atoms. Coordinates of the hydrogen atoms were calculated and included in the refinement constrained to C–H and N–H bond lengths of 0.96 Å and to an idealized geometry. Isotropic thermal parameters of the hydrogen atoms were fixed at 1.2 times the equivalent isotropic thermal parameter of the atom to which they are bonded. Since intensity statistics suggest the space group is centrosymmetric, final refinement of the structure occurred in space group $P\bar{1}$. Final refinement of 233 least-squares parameters gave $R$ = 0.0292 and $R_w$ = 0.0393 (0.0321 and 0.0396, respectively, for all data). Excursions on the final electron-density difference map range from −0.438 to 0.367 e/Å$^3$ (maximum is 0.75 Å from Cu(2)). Atomic coordinates are reported in Table II; bond lengths and angles are reported in Tables III and IV. An ORTEP plot

(7) Sheldrick, G. *SHELXTL, Version 5.1*; Nicolet Analytical Instruments: Madison, WI, 1984.

**Table II.** Atomic Coordinates (×10$^4$) and Equivalent Isotropic Thermal Parameters (Å$^2$ × 10$^3$) for $(1,4\text{-DMP})_4Cu_5Cl_{14}$ (I) and $(ETrMA)_4Cu_5Cl_{14}$ (II)

| atom | $x$ | $y$ | $z$ | $U_{eq}$[a] |
|---|---|---|---|---|
| | | I | | |
| Cu(1) | 0 | 0 | 0 | 34 (1) |
| Cu(2) | 72 (1) | 3363 (1) | 279 (1) | 29 (1) |
| Cu(3) | 852 (1) | 2161 (1) | 2891 (1) | 27 (1) |
| Cl(1) | 2063 (1) | 1997 (1) | −97 (1) | 35 (1) |
| Cl(2) | −2088 (1) | 1365 (1) | 103 (1) | 31 (1) |
| Cl(3) | −2136 (1) | 4635 (1) | −204 (1) | 34 (1) |
| Cl(4) | 197 (1) | 3714 (1) | 1913 (1) | 35 (1) |
| Cl(5) | 1053 (1) | 421 (1) | 1905 (1) | 39 (1) |
| Cl(6) | 3326 (1) | 2236 (1) | 3871 (1) | 45 (1) |
| Cl(7) | −1070 (1) | 2558 (1) | 3816 (1) | 44 (1) |
| N(1) | 6539 (4) | 5060 (3) | 2440 (2) | 36 (1) |
| C(2) | 7316 (5) | 6121 (4) | 2040 (3) | 46 (1) |
| C(3) | 8349 (5) | 7291 (4) | 2537 (3) | 41 (1) |
| C(4) | 8593 (5) | 7394 (3) | 3459 (2) | 36 (1) |
| C(5) | 7803 (5) | 6272 (4) | 3854 (3) | 45 (1) |
| C(6) | 6771 (5) | 5107 (4) | 3327 (3) | 41 (1) |
| C(7) | 5434 (6) | 3819 (4) | 1878 (3) | 56 (2) |
| C(8) | 9664 () | 8686 (4) | 4006 (3) | 53 (1) |
| N(11) | 5073 (4) | 839 (3) | 7510 (2) | 37 (1) |
| C(12) | 4706 (5) | 550 (4) | 6611 (3) | 44 (1) |
| C(13) | 5369 (5) | 1499 (4) | 6074 (3) | 46 (1) |
| C(14) | 6440 (5) | 2769 (4) | 6428 (2) | 37 (1) |
| C(15) | 6827 (5) | 2999 (4) | 7355 (3) | 43 (1) |
| C(16) | 6122 (5) | 2030 (4) | 7867 (3) | 44 (1) |
| C(17) | 4307 (6) | −168 (4) | 8092 (3) | 56 (2) |
| C(18) | 7143 (6) | 3824 (4) | 5842 (3) | 53 (2) |
| | | II | | |
| Cu(1) | 0 | 5000 | 0 | 33 (1) |
| Cu(2) | −24 (1) | 4568 (1) | 1981 (1) | 35 (1) |
| Cu(3) | 191 (1) | 5136 (1) | 3954 (1) | 35 (1) |
| Cl(1) | 650 (1) | 6324 (2) | 1113 (1) | 38 (1) |
| Cl(2) | −452 (1) | 6487 (2) | 2866 (1) | 43 (1) |
| Cl(3) | 1521 (1) | 5246 (2) | 3418 (1) | 47 (1) |
| Cl(4) | 510 (1) | 2697 (2) | 1210 (1) | 44 (1) |
| Cl(5) | 624 (1) | 3656 (2) | 5073 (1) | 61 (1) |
| Cl(6) | −472 (1) | 2994 (2) | 3030 (1) | 45 (1) |
| Cl(7) | 1255 (1) | 5015 (2) | −738 (1) | 42 (1) |
| N(1) | 1662 (3) | −137 (4) | 3448 (3) | 36 (1) |
| C(11) | 2459 (3) | −1034 (6) | 3585 (4) | 45 (1) |
| C(12) | 1278 (4) | −491 (8) | 2583 (4) | 65 (2) |
| C(13) | 1893 (4) | 1460 (6) | 3491 (4) | 66 (2) |
| C(14) | 1005 (4) | −523 (7) | 4088 (4) | 59 (2) |
| C(15) | 1292 (4) | −331 (7) | 5017 (4) | 67 (2) |
| N(2) | 1755 (3) | 108 (5) | 9079 (3) | 46 (1) |
| C(21) | 2373 (5) | 1307 (8) | 9325 (6) | 103 (2) |
| C(22)[b] | 1683 (9) | −857 (13) | 9877 (7) | 103 (2) |
| C(23)[b] | 850 (5) | 707 (11) | 8910 (7) | 68 (2) |
| C(24)[b] | 2069 (7) | −811 (13) | 8424 (7) | 91 (2) |
| C(25) | 2102 (6) | 116 (11) | 7537 (5) | 115 (2) |
| C(26)[c] | 1073 (11) | 197 (21) | 9679 (10) | 104 (2) |
| C(27)[c] | 2118 (13) | −1412 (14) | 9102 (10) | 77 (2) |
| C(28)[c] | 1387 (12) | 340 (19) | 8204 (7) | 89 (2) |

[a] Equivalent isotropic $U$ defined as one-third of the trace of the orthogonalized $U_{ij}$ tensor. [b] Site occupation factor = 0.6921. [c] Site occupation factor = 0.3079.

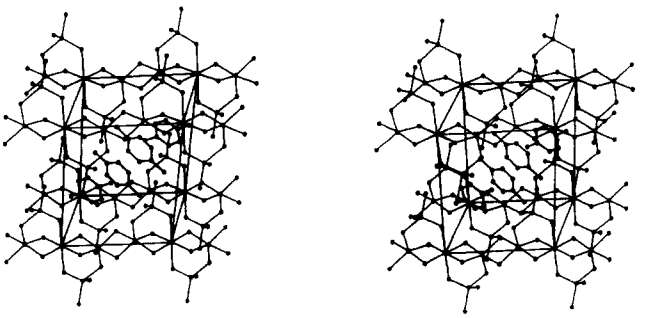

**Figure 2.** Stereoscopic packing diagram of $(1,4\text{-DMP})_4Cu_5Cl_{14}$. The box outlines the boundaries of one unit cell with the $a$ axis into the plane of the paper, $b$ axis horizontal, and $c$ axis vertical.

**Table III.** Cu–Cl Bond Lengths (Å) for $(1,4\text{-DMP})_4Cu_5Cl_{14}$ (I) and $(ETrMA)_4Cu_5Cl_{14}$ (II)

| | | | |
|---|---|---|---|
| | | I | |
| Cu(1)–Cl(1) | 2.305 (1) | Cu(1)–Cl(2) | 2.302 (1) |
| Cu(1)–Cl(5) | 2.868 (1) | Cu(2)–Cl(1) | 2.323 (1) |
| Cu(2)–Cl(2) | 2.287 (1) | Cu(2)–Cl(3) | 2.382 (1) |
| Cu(2)–Cl(4) | 2.456 (1) | Cu(2)–Cl(3A) | 2.301 (1) |
| Cu(3)–Cl(4) | 2.316 (1) | Cu(3)–Cl(5) | 2.236 (1) |
| Cu(3)–Cl(6) | 2.229 (1) | Cu(3)–Cl(7) | 2.216 (1) |
| | | II | |
| Cu(1)–Cl(1) | 2.313 (1) | Cu(1)–Cl(4) | 2.907 (2) |
| Cu(1)–Cl(7) | 2.308 (1) | Cu(2)–Cl(1) | 2.367 (2) |
| Cu(2)–Cl(2) | 2.338 (2) | Cu(2)–Cl(4) | 2.261 (2) |
| Cu(2)–Cl(6) | 2.308 (2) | Cu(2)–Cl(7A) | 2.694 (2) |
| Cu(3)–Cl(2) | 2.291 (2) | Cu(3)–Cl(3) | 2.263 (2) |
| Cu(3)–Cl(5) | 2.286 (2) | Cu(3)–Cl(6) | 2.606 (2) |
| Cu(3)–Cl(5B) | 2.302 (2) | | |

**Table IV.** Cl–Cu–Cl and Cu–Cl–Cu Bond Angles (deg) for $(1,4\text{-DMP})_4Cu_5Cl_{14}$ (I) and $(ETrMA)_4Cu_5Cl_{14}$ (II)[a]

| | | | |
|---|---|---|---|
| | | I | |
| Cl(1)–Cu(1)–Cl(2) | 86.3 (1) | Cl(1)–Cu(1)–Cl(5) | 88.4 (1) |
| Cl(2)–Cu(1)–Cl(5) | 90.9 (1) | Cl(1)–Cu(2)–Cl(2) | 86.2 (1) |
| Cl(1)–Cu(2)–Cl(3) | 148.3 (1) | Cl(2)–Cu(2)–Cl(3) | 91.5 (1) |
| Cl(1)–Cu(2)–Cl(4) | 110.4 (1) | Cl(2)–Cu(2)–Cl(4) | 94.3 (1) |
| Cl(3)–Cu(2)–Cl(4) | 101.3 (1) | Cl(1)–Cu(2)–Cl(3A) | 92.6 (1) |
| Cl(2)–Cu(2)–Cl(3A) | 170.5 (1) | Cl(3)–Cu(2)–Cl(3A) | 84.6 (1) |
| Cl(4)–Cu(2)–Cl(3A) | 94.9 (1) | Cl(4)–Cu(3)–Cl(5) | 99.6 (1) |
| Cl(4)–Cu(3)–Cl(6) | 130.3 (1) | Cl(5)–Cu(3)–Cl(6) | 99.8 (1) |
| Cl(4)–Cu(3)–Cl(7) | 96.2 (1) | Cl(5)–Cu(3)–Cl(7) | 136.2 (1) |
| Cl(6)–Cu(3)–Cl(7) | 100.3 (1) | Cu(1)–Cl(1)–Cu(2) | 92.3 (1) |
| Cu(1)–Cl(2)–Cu(2) | 93.3 (1) | Cu(2)–Cl(3)–Cu(2A) | 95.4 (1) |
| Cu(2)–Cl(4)–Cu(3) | 125.1 (1) | Cu(1)–Cl(5)–Cu(3) | 129.5 (1) |
| | | II | |
| Cl(1)–Cu(1)–Cl(4) | 77.5 (1) | Cl(1)–Cu(1)–Cl(7) | 91.5 (1) |
| Cl(4)–Cu(1)–Cl(7) | 97.0 (1) | Cl(1)–Cu(2)–Cl(2) | 89.2 (1) |
| Cl(1)–Cu(2)–Cl(4) | 90.8 (1) | Cl(2)–Cu(2)–Cl(4) | 174.3 (1) |
| Cl(1)–Cu(2)–Cl(6) | 168.5 (1) | Cl(2)–Cu(2)–Cl(6) | 86.2 (1) |
| Cl(4)–Cu(2)–Cl(6) | 92.7 (1) | Cl(1)–Cu(2)–Cl(7A) | 78.8 (1) |
| Cl(2)–Cu(2)–Cl(7A) | 96.6 (1) | Cl(4)–Cu(2)–Cl(7A) | 89.0 (1) |
| Cl(6)–Cu(2)–Cl(7A) | 112.2 (1) | Cl(2)–Cu(3)–Cl(3) | 94.2 (1) |
| Cl(2)–Cu(3)–Cl(5) | 171.2 (1) | Cl(3)–Cu(3)–Cl(5) | 94.0 (1) |
| Cl(2)–Cu(3)–Cl(6) | 80.6 (1) | Cl(3)–Cu(3)–Cl(6) | 99.8 (1) |
| Cl(5)–Cu(3)–Cl(6) | 94.9 (1) | Cl(2)–Cu(3)–Cl(5B) | 90.4 (1) |
| Cl(3)–Cu(3)–Cl(5B) | 139.6 (1) | Cl(5)–Cu(3)–Cl(5B) | 85.5 (1) |
| Cl(6)–Cu(3)–Cl(5B) | 120.6 (1) | Cu(1)–Cl(1)–Cu(2) | 84.1 (1) |
| Cu(2)–Cl(2)–Cu(3) | 85.4 (1) | Cu(1)–Cl(4)–Cu(2) | 73.5 (1) |
| Cu(3)–Cl(5)–Cu(3B) | 94.5 (1) | Cu(2)–Cl(6)–Cu(3) | 79.2 (1) |
| Cu(1)–Cl(7)–Cu(2A) | 77.2 (1) | | |

[a] Symmetry key: A, $(-x, 1-y, -z)$; B, $(-x, 1-y, 1-z)$.

of part of the structure is presented in Figure 1, and a stereographic packing diagram of the structure is presented in Figure 2.

**$(ETrMA)_4Cu_5Cl_{14}$.** Ethyltrimethylammonium chloride was prepared by reacting equimolar amounts of ethyldimethylamine with chloromethane. Single crystals of the copper chloride salt were grown by slow evaporation of a concentrated HCl solution initially equimolar in ethyltrimethylammonium chloride and copper(II) chloride. The scarlet crystals deform on cutting; however, a specimen small enough for structure determination was easily found.

X-ray diffraction data were collected on the instrument described previously. Cell constants were determined by a least-squares refinement of the angular settings of 25 well-centered reflections occurring in the range $35° < 2\theta < 37°$.[6] Pertinent details of the data collection are listed in Table I. Intensities of three check reflections were measured every 93 reflections, variations within counting statistics. Lorentz–polarization and crystal decay corrections were applied to the data. An empirical absorption correction assuming an ellipsoidal crystal shape was also applied. Systematic absences unambiguously identify the space group as $P2_1/n$. Structure solution and refinement were achieved via the Nicolet SHELXTL package.[7] Coordinates of several of the heavy atoms were found on the $E$ map calculated from direct methods, while the coordinates for the remaining non-hydrogen atoms were identified from subsequent electron-density difference maps. Anomalously large thermal parameters and large difference map peaks during the refinement indicated a 2-fold disorder of cation 2. The two conformations of cation 2 are roughly related by a hypothetical mirror plane defined by the N(2), C(21), and C(25) atoms. The disorder was included in the refinement with site occupation factors for the disordered pair refined with the constraint that their sum equal 1.0. Refinement at this point gave a large $R_w$ value, numerous large, randomly placed peaks about the heavy atoms on the electron-density difference map, and calculated $|F|$ values close to zero for many observed reflections. Examination of reflection peak scans revealed a slight asymmetry or off-center intensity in several, suggesting the presence of a small twin. Data were reduced again, this time severely tightening the reflection rejection criteria, resulting in the systematic rejection of 272 reflections. Hydrogen atoms were not visible on the difference map, but their coordinates were calculated for cation 1 and the dominant cation 2 orientation. The cation 1 hydrogen atom coordinates were refined with a riding model that constrained the C–H bond distance to 0.96 Å and the coordinates to an idealized geometry, while the cation 2 hydrogen atom coordinates were fixed through the remaining cycles of refinement. Anisotropic thermal parameters were refined for all non-hydrogen atoms, and isotropic thermal parameters for the hydrogen atoms were fixed at 1.2 times the equivalent isotropic thermal parameter of the atoms to which they are bonded. Final refinement of 225 least-squares parameters yielded $R = 0.0526$ and $R_w = 0.0455$ (0.0808 and 0.0508, respectively, for all data). Excursions on the final electron-density difference map range from −0.531 to 0.718 e/Å$^3$. Atomic coordinates are reported in Table II; bond lengths and bond angles are reported in Tables III and IV. An ORTEP plot of the chain structure is presented in Figure 3; a stereographic packing diagram of the unit cell is presented in Figure 4.

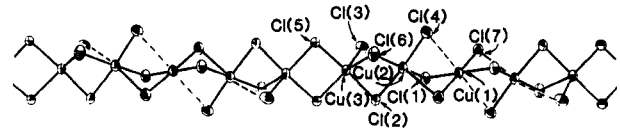


**Figure 3.** View of the chain structure in $(ETrMA)_4Cu_5Cl_{14}$. Dashed lines indicate semicoordinate Cu–Cl bonds.

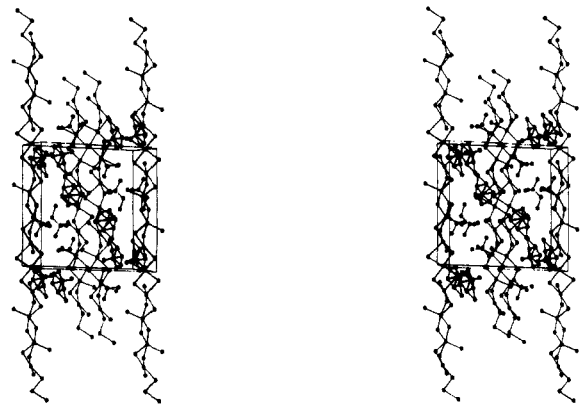

**Figure 4.** Stereoscopic packing diagram of the $(ETrMA)_4Cu_5Cl_{14}$ structure. The box outlines the boundaries of one unit cell with the $a$ axis horizontal, $b$ axis out of the plane of the paper, and $c$ axis vertical.

**Magnetic Susceptibility Data.** Data for both compounds were collected on PAR 152 vibrating sample magnetometers. Magnetic moment data (77 points) were collected in the temperature range 2–100 K on a 0.1864-g powdered sample of $(1,4\text{-DMP})_4Cu_5Cl_{14}$ in a field of 9870 G. Magnetic moments were corrected for a small background moment (−0.0002 emu) and multiplied by an instrument operation correction of 3.91715. The latter factor was obtained by dividing the known saturation moment of a small nickel sphere with that measured by the magnetometer. Assuming linear behavior of the magnetization at the measured field, the magnetic susceptibility may be calculated with the expression $\chi(H = 0) = M/H$. Molar susceptibilities were calculated from the raw susceptibility data corrected for diamagnetism (−0.000 722 64 emu/mol)[8] and temperature-independent paramagnetism (0.000 300 emu/mol). Magnetic moment data were collected in the temperature range 4.2–80 K on a 0.0900-g powdered sample of $(ETrMA)_4Cu_5Cl_{14}$ in a field of 5000 G. Magnetization curves at 4.2 and 15 K were linear to 5000 G; thus, the susceptibility was calculated as described previously (no instrument correction, corrections for diamagnetism, −0.000 725 28 emu/mol, and temperature-independent paramagnetism, 0.000 300 emu/mol).

(8) Selwood, P. W. *Magnetochemistry*, 2nd ed.; Interscience: New York, 1956; p 78.

**Structure Descriptions**

**(1,4-DMP)$_4$Cu$_5$Cl$_{14}$.** The crystal structure consists of discrete 1,4-dimethylpyridinium cations and infinite $(Cu_5Cl_{14}^{4-})_n$ "knobby" chains. Within the chains (Figure 1), three distinct coordination sites exist: Cu(1), at a site of $\bar{1}$ symmetry, with a 4 + 2 coordination geometry ($(Cu-Cl)_{av}$ = 2.303 (1) Å, Cu···Cl = 2.868 (1) Å); Cu(2) with a distorted square-pyramidal geometry ($(Cu-Cl_{bas})_{av}$ = 2.32 (4) Å, $Cu-Cl_{ax}$ = 2.456 (1) Å, *trans*-$Cl_{bas}$–Cu–$Cl_{bas}$ = 170.5 (1) and 148.3 (1)°); Cu(3) with a distorted tetrahedral coordination geometry ($(Cu-Cl)_{av}$ = 2.250 (5) Å, *trans*-Cl–Cu–Cl = 136.2 (1) and 130.3 (1)°). The chain itself consists of repeating Cu(1)–Cu(2)–Cu(2) sequences, each adjacent pair of copper ions linked by two symmetrical Cu–Cl–Cu bridges. The configuration of the Cu(2)–Cu(2) linkage is very close to that observed in a series of stacked bifolded $Cu_2Cl_6^{2-}$ dimers,[9] while the Cu(2)–Cu(1)–Cu(2) grouping has a conformation closer to that observed in stacked, planar $Cu_3Cl_8^{2-}$ trimers.[10] The tetrahedra associated with the Cu(3) ions form the "knobs" on the chains, bridging between neighboring Cu(1) and Cu(2) ions in the trimeric unit. These linkages between the tetrahedral copper ion and the copper ions in the chain involve a symmetrical bridge to Cu(2) and an asymmetrical bridge to Cu(1).

Associated with the $Cu_5Cl_{14}^{4-}$ cluster described above are two pairs of crystallographically inequivalent 1,4-DMP cations. The inequivalent cations are almost coplanar with a 1° difference between the normals to their planes; however, one cation lies at an angle of 69° from an eclipsed configuration with the other. Both cations form long N···Cl interactions with the bridging chloride ions of the tetrahedral copper species with contact distances (N(1)···Cl(4) = 3.474 Å, N(11)···Cl(5) = 3.475 Å) and interaction vector angles (12.2° for cation 1 and 15.2° for cation 2 measured with respect to the normal to the cation plane) that are comparable in length and direction to those observed in other quaternary pyridinium halometalates.[11]

The long-range structure of the crystal may be described as layers of knobby chains parallel to the *ab* plane stacked atop one another. Neighboring $Cu_5Cl_{14}^{4-}$ clusters in the chain are related by an inversion center located between neighboring five-coordinate copper ions and by a *b*-axis lattice translation. The chain axis, then, is parallel to the *b* axis of the crystal with the knobs on the chains extending out of the *ab* plane of the crystal. The closest interchain chloride–chloride contacts (4.22 Å) are found between the nonbridging chloride ions, Cl(6) and Cl(7). The line through Cl(6) and Cl(7) is approximately parallel to the *a* axis. As a result, the nonbridging chlorides of one chain contact those of two neighboring chains along the *a* axis, defining the layers of the structure, with the knobs on the chains extending above and below this layer. The coplanar cations are stacked in pairs between these chains inside a cavity bounded by two pairs of knobs on neighboring chains in the layer. The cations in the cavity are crystallographically inequivalent and are rotated relative to one another (vide infra), reducing steric effects between their methyl groups. Methyl groups of the cations extend out of the layer, effectively separating neighboring layers, while the knobs on neighboring layers are staggered relative to each other so as to minimize the interlayer distance.

The application of the charge compensation ideas to this structure is quite straightforward. The chloride ions involved in the symmetric bridges find electrostatic repulsion reduced to the point where the crystal field stabilization energy dominates. Thus, Cu(1) assumes a planar configuration, allowing for the formation of two semicoordinate bonds, while Cu(2) takes on a square-pyramidal conformation. Of the chloride ions bonded to Cu(3), two are involved in bridge formation (one symmetric, one asymmetric). The other two are involved in no direct charge compensation mechanisms, their only contacts are with the 1,4-DMP cations. Thus, the coordination geometry is dominated by the electrostatic repulsions between the halide ions, and only a small distortion from a tetrahedral geometry is observed.

**(ETrMA)$_4$Cu$_5$Cl$_{14}$.** The structure consists of linear chains of $Cu_5Cl_{14}^{4-}$ pentamers with the chains isolated from one another by the bulky ETrMA cations. The pentameric unit of the inorganic chain has inversion symmetry and contains copper ions in three distinct coordination geometries, as in the previously described structure. The pentamer in this case, however, is linear, in contrast to the "bowtie" configuration in the other structure. The central copper ion of the pentamer sits on a center of inversion and exhibits a distorted octahedral coordination geometry with all equatorial Cu–Cl bond lengths almost identical ($(Cu-Cl_{eq})_{av}$ = 2.311 (3) Å, $Cu-Cl_{ax}$ = 2.907 (2) Å). The two other crystallographically independent copper(II) ions of the pentamer both exhibit distorted square-pyramidal geometries; however, the amount of distortion is very different in the two cases. The coordination geometry about Cu(2) is close to square pyramidal (Cu(2) also forms a long, semicoordinate bond with Cl(3), 3.273 Å, so the actual geometry is 4 + 1 + 1′), with $(Cu-Cl_{bas})_{av}$ = 2.32 (5) Å and $Cu-Cl_{ax}$ = 2.694 (2) Å. The major distortions of the square pyramid result from elongation of the chain caused by intrachain cation–cation repulsion. The geometry about Cu(3) is strongly distorted toward trigonal bipyramidal. The Cu–Cl bond lengths are similar to those about Cu(2). $(Cu-Cl_{bas})_{av}$ = 2.29 (2) Å and $Cu-Cl_{ax}$ = 2.606 (2) Å; however, one of the basal chlorides is distorted out of the plane formed by the other three basal ligands, forming an angle of 139.6 (1)° with the axial chloride. Thus, one may easily discern a nascent trigonal bipyramid with Cl(3), Cl(6), and Cl(5a) (related to Cl(5) by inversion) defining the equatorial plane and Cl(5) and Cl(2) defining the trigonal axis.

The copper ions of the chain are linked together by both symmetric and asymmetric bridges. Each copper ion within the pentamer is linked to its neighbor by one symmetric and two asymmetric bridges, as is found in the series of tribridged $(CuCl_3)_n$ chains.[4] Two symmetric bridges between adjacent Cu(3) atoms (related by inversion) form the linkages between pentamers, which complete the linear chain structure. Intrachain repulsion between the metal cations results in an elongation of the chain, which is manifest by acute, internal Cl–Cu–Cl angles.

Since all chloride ions are involved in bridges between copper ions, one can understand why, on the basis of charge compensation arguments, the tetrahedral geometry is absent from the chain. The inversion center about Cu(1) favors the observed 4 + 2 geometry, while the presence of the distant axial chloride in the 4 + 1 + 1′ geometry of Cu(2) prevents distortion of any of the basal chlorides out of the plane preserving the square-pyramidal geometry. Cu(3), on the other hand, exhibits a severe distortion of the square-pyramidal geometry, and its coordination sphere is best described as intermediate between square pyramidal and trigonal bipyramidal. The cause of these differences in geometry of the copper(II) ions is certainly more complex than can be treated by the crude "charge compensation" ideas. In the absence of a more complete theory, we must attribute these differences to "packing forces".

Two chloride bridges between square-pyramidal copper(II) ions link the pentameric units in the chain, as in the 1,4-DMP salt. Adjacent pentameric units in the chain are related by inversion, and the chain axes correspond to the lines of inversion centers parallel to the *c* axis. Each chain is related to four nearest neighbors by an *n* glide or a $2_1$ rotation (interchain distance = 8.970 Å), while two others are related by a *b*-axis translation. The closest interchain chloride–chloride contacts arise between chains related by the *n* glide or $2_1$ rotation (Cl(3)–Cl(4a) = 5.12 Å, Cl(3)–Cl(1a) = 5.67 Å; $a = {}^1/_2 - x, {}^1/_2 + y, {}^1/_2 - z$); chloride–chloride contacts between chains related by a *b*-axis translation are all greater than 5.78 Å. The chains related by the *n* glide or $2_1$ rotation are, of course, staggered with the central copper ion of the pentameric unit of one chain on the same level as the bridges between pentamers in the four nearest-neighbor chains.

The inorganic chains are separated by the bulky ethyltrimethylammonium cations. As noted in the experimental section,

(9) Scott, B.; Willett, R. *Inorg. Chim. Acta* **1988**, *141*, 193–199.
(10) Grigereit, T. E.; Ramakrishna, B. L.; Place, H.; Willett, R. D.; Pellacani, G. C.; Manfredini, T.; Menabue, L.; Bonamartini-Corradi, A.; Battaglia, L. P. *Inorg. Chem.* **1987**, *26*, 2235–2243.
(11) Prout, C. K.; Murray-Rust, P. *J. Chem. Soc. A* **1969**, 1520–1525.

**Table V.** Spin and Symmetry Properties of the Bowtie Cluster Eigenstates

| spin ($S$) | $2S + 1$ | gerade | ungerade | tot. levels |
|---|---|---|---|---|
| $^5/_2$ | 6 | 1 | 0 | 1 |
| $^3/_2$ | 4 | 2 | 2 | 4 |
| $^1/_2$ | 2 | 3 | 2 | 5 |

**Table VI.** Energy of Bowtie Cluster Levels in Zero Field

$E(S = {}^5/_2) = -(J_{12} + J_{13} + J_{23})$
$E(S = {}^3/_2, u) = -{}^1/_2\{(J_{12} + J_{13}) \pm [(J_{12} - J_{13})^2 + 4J_{23}^2]^{1/2}\}$
$E(S = {}^3/_2, g) = {}^1/_2\{(J_{12} + J_{13}) \mp [9(J_{12}^2 + J_{13}^2) - 2J_{12}J_{13} - 8J_{23}(J_{12} + J_{13}) + 4J_{23}^2]^{1/2}\}$
$E(S = {}^1/_2, u) = (J_{12} + J_{13}) \pm [(J_{12} - J_{13})^2 + J_{23}^2]^{1/2}$
$E(S = {}^1/_2, g)$: $E^3 - (3J_{23} + J_{12} + J_{13})E^2 - [J_{23}^2 - 2J_{23}(J_{12} + J_{13}) + 2(J_{12} - J_{13})^2]E + 3J_{23}^2(J_{23} + J_{13} + J_{12}) = 0$

one of the two crystallographically inequivalent cations exhibits 2-fold disorder with the ethyl groups of the cation assuming a staggered conformation in both cases. The cations form columns parallel to the inorganic chains, in which the ordered and disordered cations alternate, with each inorganic chain surrounded by six of these columns. This segregates the cations into layers, corresponding to the {202} family of crystal planes, in which layers of ordered cations alternate with layers of disordered cations.

## Magnetic Model

Since the inorganic portion of these compounds is described structurally as chains of pentamers, an appropriate model for the magnetic susceptibility would first consider an expression for the isolated pentanuclear cluster and then account for the intercluster interaction through a mean field approximation. An examination of the susceptibility data shows that the intercluster interaction is small, and it was felt that this approach would be useful. The model spin Hamiltonian for the isolated cluster takes the form $H = -2J_{12}(\vec{S}_1\cdot\vec{S}_2 + \vec{S}_1\cdot\vec{S}_{2a}) - 2J_{13}(\vec{S}_1\cdot\vec{S}_3 + \vec{S}_1\cdot\vec{S}_{3a}) - 2J_{23}(\vec{S}_2\cdot\vec{S}_3 + \vec{S}_{2a}\cdot\vec{S}_{3a}) + g\mu_B H\sum_i S_i^z$, which reflects the inversion symmetry of the model cluster (the bowtie cluster) shown in diagram I.

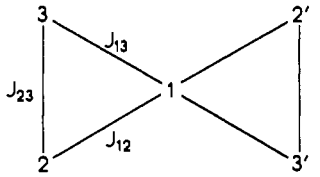


I

A few simplifying assumptions are made in writing the model spin Hamiltonian.[12] (1) The model assumes isotropic (Heisenberg) exchange interactions; however, copper(II) halide systems typically exhibit a 1–10% exchange anisotropy. (2) Isotropic $g$ factors are assumed, although anisotropic $g$ factors are expected. (3) Magnetically inequivalent ions are assumed to have the same average $g$ factor. Since the three inequivalent ions have widely variant coordination geometries, this is unlikely. These factors, however, represent small changes in the magnetic properties of the system; hence, the powder susceptibility data should be insensitive to them.

The symmetry of the Heisenberg Hamiltonian allows the eigenstates to be labeled according to the value of the total spin, $S$. In zero magnetic field the states will also be grouped into $(2S + 1)$-degenerate levels. The states (and, hence, the levels) may be further classified according to their symmetry or antisymmetry (gerade or ungerade) with respect to inversion. The breakdown of the levels by total spin, $S$, and their behavior under inversion is presented in Table V. From the table it is obvious that the largest Hamiltonian matrix that need be diagonalized has a dimension of 3, hence, precise expressions for the energies of all spin levels in zero field can be obtained and are listed in Table VI except for the energies of the symmetric, $S = {}^1/_2$ levels. The energies of these levels are roots of a cubic equation whose coefficients are

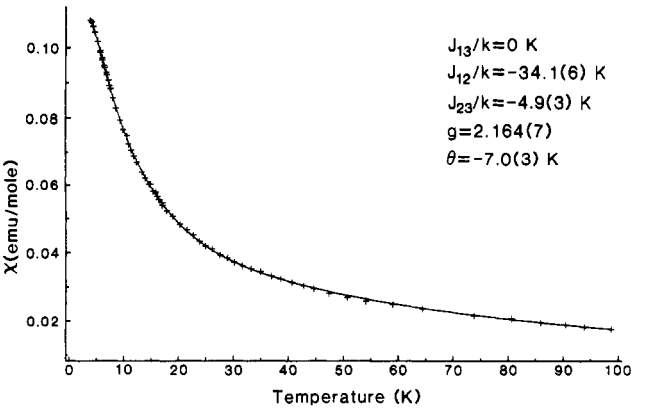


**Figure 5.** Plot of the experimental magnetic susceptibility (+) and the best fit curve (—) versus temperature for $(1,4\text{-DMP})_4Cu_5Cl_{14}$.

complicated expressions of the exchange parameters, so the exact expressions for the energies may only be obtained following lengthy algebraic manipulation. It is easier, instead, to work directly with the cubic equation listed in Table VI.

The expression for the cluster susceptibility is obtained by application of van Vleck's equation:

$$\chi_{cluster} = \frac{N\sum_n[(E_n^{(1)})^2/kT]\exp(-E_n^\circ/kT)}{\sum_n \exp(-E_n^\circ/kT)}$$

where $N$ is Avogadro's number, $E_n^{(1)} = m_s g\mu_B$, and $E_n^\circ$ is the energy of the $n$th spin state in zero field.[13] The mean field corrected susceptibility takes the form

$$\chi' = \chi_{cluster}\Big/\left(1 - \frac{2zJ'}{Ng\mu_B{}^2}\chi_{cluster}\right)$$

where $z$ is the number of neighboring clusters and $J'$ is the intercluster exchange interaction. A simpler form of the mean field correction may be used if the average spin of the cluster is constant with temperature:

$$\chi' = \chi_{cluster}(T/(T - \Theta))$$

where $\Theta = 2S(S + 1)zJ'/3k$.[14]

## Magnetic Results

The susceptibility data for the two compounds are plotted in Figures 5 and 6a. In both cases the susceptibility reaches a maximum at low temperature. Data for the 1,4-DMP salt have been collected below liquid-helium temperature (lack of a precise temperature calibration in this range prevents inclusion of the data) and show a maximum in the susceptibility at approximately 3.7 K. Since all cluster eigenstates possess a nonzero spin, one would expect the susceptibility of a collection of isolated clusters to diverge as the temperature approaches 0 K. The presence of a maximum in the susceptibility, then, indicates an antiferromagnetic interaction between neighboring clusters in the chain. A plot of $\chi T$ versus $T$ indicates generally antiferromagnetic intracluster interactions for the 1,4-DMP salt, while the opposite is true for the EtTrMA salt. At high temperature the value of $\chi T$ for both compounds asymptotically approaches the paramagnetic limit ($\chi T \approx 2.15$ emu/(K mol)). In the 1,4-DMP salt the value of $\chi T$ decreases monotonically to zero as $T$ goes to 0 K. In the EtTrMA salt $\chi T$ increases to a maximum of 2.8 emu/(K mol) at 30 K and then decreases monotonically to zero as $T$ goes to 0 K. The magnetic susceptibility versus temperature curves for both compounds were fit to the theoretical model described above.

All parameters of the model were refined initially for the 1,4-DMP salt. The error in the resulting best-fit parameters was very large, with the error for the smallest parameter, $J_{13}/k \approx 0.9$, almost 30 times its magnitude. The value of $J_{13}$ was then fixed at zero and the model refined again, resulting in much smaller

(12) Willett, R. D. In *Magneto-Structural Correlations in Exchange Coupled Systems*; Willett, R. D., Gatteschi, D., Kahn, O., Eds.; Plenum: New York, 1985; pp 394–397.

(13) Carlin, R. L. *Magnetochemistry*; Springer-Verlag: Berlin, 1986; pp 8–9.

(14) Ginsberg, A. P.; Lines, M. E. *Inorg. Chem.* **1967**, *6*, 2289–2290.

**Table VII.** Summary of Stereochemistries in Copper(II) Halide Salts with Multiple Stereochemistries

| compd | stereochemistry[a] | bridging halides[b] | N-H···X contacts[c] | ref |
|---|---|---|---|---|
| $[(C_2H_5)_4N]_4Cu_4Cl_{12}$ | 4 + 1 (2.662 Å, tet) | 3,1 | 0 | 16 |
| | 4 (141.4°) | 2 | 0 | |
| [*N*-(2-ammonioethyl)piperazinium]$_4Cu_5Cl_{22}$ | 4 + 2 (2.971 Å) | 0,2 | 4 | 17 |
| | 4 + 1 (2.719 Å, sp) | 0,1 | 4 | |
| | 4 (125.6°) | 0 | 0 | |
| | 4 (141.8°) | 0 | 0 | |
| $[(C_2H_5)_2NH_2]_2CuCl_4$ (room temp) | 4 (145°) | 0 | | 18 |
| | 4 (159°) | 0 | | |
| | 4 (178°) | 0 | | |
| (*N*-benzylpiperazinium)$_2CuCl_4$ | 4 (137°) | 0 | 3 | 19 |
| | 4 (151°) | 0 | 3 | |
| $(CuL_3)_2Cu_2Cl_6$ (L = $(Ph_2PO)_2CH_2$) | 4 (124.8°) | 2 | 0 | 20 |
| | 4 (143.2°) | 2 | 0 | |
| $[(CH_3)_2CHNH_3]_2CuCl_4$ (room temp) | 4 + 2 (3.070, 3.103 Å) | 2,2 | (8,8)[d] | 21 |
| | 4 + 1 (3.326, 3.123 Å, sp) | 1,1 | (5,6)[d] | |
| $[(C_2H_5)_2NH_2]_2Cu_3Br_8 \cdot CuBr_2 \cdot C_2H_5OH$ | 4 + 2 (3.241) Å | 4,2 | 2 | 22 |
| | 4 + 2 (3.236 Å) | 2,2 | 0 | |
| | 4 (116.9°) | 4 | 0 | |
| $[(C_2H_5)_4N]_8Cu_{14}Cl_{28}O_4$ | 5 (tbp) | 4 | 0 | 23 |
| | 4 + 1 (2.709–2.828 Å, sp) | 2,2 | 0 | |
| | 4 + 1 (3.100 Å, tet) | 3,1 | 0 | |
| (1,4-dimethylpyridinium)$_4Cu_5Cl_{14}$ | 4 + 2 (2.868 Å) | 4,2 | 0 | this work |
| | 5 (2.456 Å, sp) | 4,1 | 0 | |
| | 4 (133.2°) | 2 | 0 | |
| $(EtMe_3N)_4Cu_5Cl_{14}$ | 4 + 2 (2.907 Å) | 4,2 | 0 | this work |
| | 4 + 1 + 1 (2.694, 3.273 Å) | 4,2 | 0 | |
| | 4 + 1 (2.606 Å, sp) | 4,1 | 0 | |

[a] Axial Cu–Cl bond lengths for 4 + 2, 4 + 1, and 5 coordinate species and average *trans*-Cl–Cu–Cl bond angles for 4-coordinate species are listed. The dominate coordination geometry for 4 + 1 or 5 coordinate compounds (square pyramidal (sp), trigonal pyramidal (tbp), or tetrahedral (tet)) is also listed. [b] Listed as *m,n* pairs, where *m* is the number of normally coordinated halides involved in bridging and *n* is the number of semicoordinate halides involved in bridging. [c] Number of N···X distances less than 3.3 Å (X = Cl) or 3.4 Å (X = Br). [d] Number of N···Cl contacts to each of the two symmetrically inequivalent copper(II) chloride complexes.

relative errors in the fit parameters. The final values of the best fit parameters are $J_{13}/k = 0$, $J_{12}/k = -34.1$ (6) K, $J_{23}/k = -4.9$ (3) K, $\Theta = -7.0$ (3) K, and $g = 2.164$ (7). From the previously defined relationship, $\Theta = J_{IC} = -7.0$ K.

Initial fitting of the model to the susceptibility data of the ETrMA salt resulted in relatively large errors for all parameters also. There is generally a large uncertainty in ferromagnetic exchange constants due to coupling with the *g* factor, and the two exchange constants refined, within error, to the same value. For these reasons the model was altered by fixing *g* at 2.05 and by defining a single, common, intracluster exchange constant. Inadequacy of the mean field approximation prevented a good fit at low temperature, so the model was only fit to data measured above 15 K. Final best fit parameters are $J_{12}/k = J_{23}/k = 37.7$ (9) K and $J'/k = -1.48$ (3) K (see Figure 6a).

To better estimate the intercluster interaction, the data measured below 15 K were fit to the Fisher one-dimensional, spin-$^5/_2$ Heisenberg model.[15] The only fitted parameter was the exchange coupling $J/k$, which refined to a value of −0.867 (4) K. The *g* factor was not refined, instead runs were made with a few different values of *g*, and the value, $g = 2.2$, that gave a curve with a maximum occurring closest in temperature to the maximum in the experimental susceptibility data was chosen. A plot of the susceptibility data ($T \leq 15$ K) and the model fit versus temperature is presented in Figure 6b. This approach is not expected to be very accurate, since the clusters are not all in an $S = {}^5/_2$ level at those temperatures. From the relation $S(S+1)J' \approx s(s+1)J_{IC}$, the value of $J'$ may be scaled up to a value approximating the actual exchange interaction between the two $s = {}^1/_2$ neighbors of the chain ($J_{IC}/k \approx -10.1$ K). This crude approximation provides a beter gauge of the intercluster interaction than the mean field correction to the high-temperature data.

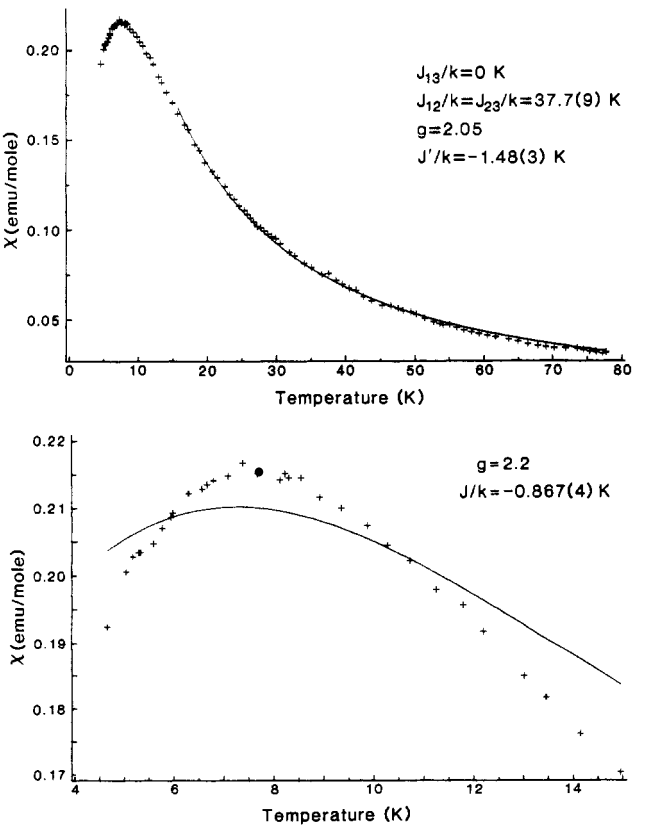


**Figure 6.** (a, Top) Plot of the experimental magnetic susceptibility (+) and the best fit curve (—) versus temperature for $(ETrMA)_4Cu_5Cl_{14}$. (b, Bottom) Plot of the experimental magnetic susceptibility data (+) and best fit curve (—) versus temperature ($T \leq 15$ °C) for $(ETrMA)_4Cu_5Cl_{14}$.

## Discussion

**Stereochemistry.** There have been several other copper(II) halide complexes reported in which two or more distinctly different coordination geometries appear in the crystal structure. These are tabulated in Table VII.[16-23] In most cases, the variation in

(15) Fisher, M. E. *Am. J. Phys.* **1964**, *32*, 343–346.

**Table VIII.** Summary of Magnetic Parameters

| pathway | exchange coupling, K | geometry | anticipated coupling |
|---|---|---|---|
| | | $(1,4\text{-DMP})_4Cu_5Cl_{14}$ | |
| $J_{12}/k$ | −34.1 (6) | sym bibridged, $\phi = 92.8°$ | AFM |
| $J_{13}/k$ | 0 | 4 + 2 axial–tet | very weak |
| $J_{23}/k$ | 4.9 (3) | 5-coord–tet | weak |
| $J_{1C}/k$ | −7.0 (3) | bifolded, sym bibridged, $\phi = 95.4°$, $\sigma = 28.6°$ | FM |
| | | $(EtTrMA)_4Cu_5Cl_{14}$ | |
| $J_{12}/k$ | 37.7 (9) | tribridged | FM |
| $J_{13}/k$ | 0 | nonbridged | zero |
| $J_{23}/k$ | 37.7 (9) | folded, sym bibridged $\phi = 85.4°$ | FM |
| $J_{1C}/k$ | ≈−10 | bifolded, sym bibridged, $\phi = 94.5°$, $\sigma = 41.4°$ | FM |

stereochemistry involves a change in coordination number, but in several instances, only a change in extent of distortion of the four-coordination occurs. For systems with little or no hydrogen-bonding capabilities, bridge formations dominate. Thus, qualitative charge compensation ideas may be used to interpret the main features of the structural results, while at the same time pointing out some of their limitations. In general, for each compound in Table VII the distortion toward tetrahedral geometry is largest for the Cu atom with the fewest bridging and/or hydrogen-bonding interactions. In particular, because of the flatness of the potential surfaces, the ever ubiquitous packing forces will certainly dominate in some cases, such as in $CuL_3Cu_2Cl_6$ in Table VII, where the tetrahedral distortion for the two separate Cu atoms in the $Cu_2Cl_6^{2-}$ dimer are distinctly different.[20]

**Magneto-Structural Correlations.** The interpretation of the magnetic parameters in terms of the geometrical structures is relatively straightforward, when comparison is made with the results for previously studied copper(II) chloride systems. Reference to the tabulation in Table VIII will be useful in this regard. The only problem encountered will be with respect to the intercluster ($\theta$ or $J'$) interactions. The rationale[24] for the assignment of the exchange-coupling values in the 1,4-DMP system is as follows. The bridging geometry in the Cu(1)–Cu(2) linkage and the coordination geometry for Cu(1) are very similar to that found in a series of pseudoplanar bibridged oligomeric copper(II) halide systems. In these, the values of $J/k$ typically range from −20 to −30 K. The bridging Cu–Cl distances in this linkage are moderately short, leading to a stronger antiferromagnetic contribution to the exchange coupling, but the Cu(2) coordination geometry is intermediate between square pyramidal and trigonal bipyramidal, leading to a weakening of the exchange interaction. Thus, the value of $J_{12}/k = -34$ K is reasonable.

The Cu(1)–Cu(3) linkage involves a single chloride bridge through the axial, semicoordinate bond of Cu(1). The magnetic orbital of Cu(1) is the $d_{x^2-y^2}$ orbital in the equatorial plane, so interaction between the magnetic orbitals of Cu(1) and Cu(3) is expected to be small and the indication that $J_{13} \approx 0$ is reasonable.

The Cu(2)–Cu(3) linkage is again monobridged; however, it now involves the apical/equatorial chloride ion of the intermediate square-pyramidal/trigonal-bipyramidal geometry of Cu(2). The magnetic orbital of Cu(2), therefore, is a mixture of the $d_{x^2-y^2}$ and $d_{z^2}$ orbitals; thus, a significant portion of the Cu(2) unpaired electron density is expected to be present on the bridging chloride. If the four-coordinate Cu(3) were square planar, the magnetic orbital would be the $d_{x^2-y^2}$ orbital and one would expect a substantial delocalization of its unpaired electron onto the bridging chloride also. However, Cu(3) is subject to a large tetrahedral distortion, which may best be described by the dihedral angle between the terminal $CuCl_2$ plane and the bridging $CuCl_2$ plane. Under this twist distortion the magnetic orbital is still of $d_{x^2-y^2}$ form; however, the orbital plane now bisects the dihedral twist angle. This distortion introduces more $\pi$ character to the extended magnetic orbital of Cu(3), decreasing the overlap with the (primarily $\sigma$) extended magnetic orbital centered at Cu(2). Finally, the large Cu–Cl–Cu bridging angle should produce a large, antiferromagnetic coupling in the absence of the tetrahedral distortion. The decrease in overlap caused by the tetrahedral distortion of the Cu(3) geometry and the incomplete delocalization of the unpaired electron on Cu(2) will, however, decrease the antiferromagnetic contribution to the exchange. Hence, the value of $J_{23} = -4.9$ K is reasonable.

In the ETrMA salt, the rationale for the values of the intracluster exchange interactions is more straightforward. The Cu(1)···Cu(2) linkage has a tribridged geometry (one symmetric bridge, two asymmetric bridges) that is very similar to those found in $(CH_3)_4NCuCl_3$, $CuCl_2(TMSO)$, and $CuCl_2(DMSO)$, where the exchange parameters range from 39 to 45 K.[25,26] Similarly, the folded bibridged geometry for the Cu(2)···Cu(3) linkage is quite similar to that found in $C_5H_9NH_3CuCl_3$ and $C_6H_{11}NH_3CuCl_3$, where the exchange coupling was found to be 45–55 K.[27] Thus, the average value of $J_{12}/k$ of 38 K is very reasonable.

The intercluster exchange in both compounds is mediated by a bibridged dimeric unit similar to a widely studied class of bifolded, bibridged $Cu_2Cl_6^{2-}$ dimers.[9] Since the magnetic properties for these compounds have been mapped out for several different distortions, it was initially thought that the rationale for the value of the exchange in the intercluster dimeric bridging units would be straightforward also. The primary factor in predicting the exchange constant value is the bridging Cu–Cl–Cu bond angle (95.4° for 1,2-DMPCC and 94.6° for $(ETrMA)_4Cu_5Cl_{14}$). Distortions of the dimer from planarity can, for a given bridging bond angle, alter the exchange interaction dramatically. The most obvious nonplanar distortion of the intercluster dimeric units is the bifold distortion (rotation of a terminal chloride out of the plane of the dimer) characterized by the angle between the bent terminal Cu–Cl bond and the bridging $CuCl_2$ plane (28.6° for $(1,4\text{-DMP})_4Cu_5Cl_{14}$; 41.4° for $(ETrMA)_4Cu_5Cl_{14}$). Comparison of these bifold angles with those of several other dimeric species (with Cu–Cl–Cu bridging angles of approximately 95°) led us to predict a strongly ferromagnetic intercluster interaction ($J_{1C}/k \approx 30$–40 K) for both compounds. Since both intercluster interactions are weakly antiferromagnetic, a more complex mechanism must be found to account for the exchange coupling.

The dimeric bridges in the two compounds studied have, in contrast, *short* axial Cu–Cl bonds (2.456 Å for $(1,4\text{-DMP})_4Cu_5Cl_{14}$; 2.606 Å for $(ETrMA)_4Cu_5Cl_{14}$). These copper(II) halide complexes are true five-coordinate species with a geometry intermediate between square pyramidal and trigonal bipyramidal. This difference in coordination number might well account for the unexpected antiferromagnetic intercluster exchange. Coordination of a fifth ligand alters the character of the magnetic orbitals and changes the overlap between the magnetic orbitals, affecting the energies of the resulting molecular orbitals. It should


(16) Willett, R. D.; Geiser, U. *Inorg. Chem.* **1986**, *25*, 4558–4561.
(17) Antolini, L.; Marcotrigiano, L.; Menabue, L.; Pellacani, G. C. *J. Am. Chem. Soc.* **1980**, *102*, 5506–5510.
(18) Simonsen, S. H.; Harlow, R. L. *Am. Crystallogr. Assoc. Ser. 2* **1977**, *5* (1), Abstract HN5.
(19) Antolini, L.; Menabue, L.; Pellacani, G. C.; Saladini, M.; Marcotrigiano, G.; Porzio, W. *J. Chem. Soc., Dalton Trans.* **1981**, 1753–1758.
(20) Yatsimirskii, K. B.; Struchkov, Yu. T.; Batsanov, A. S.; Sinyavskaya, E. I. *Koord. Khim.* **1985**, *11*, 826–832.
(21) (a) Anderson, D. N.; Willett, R. D. *Inorg. Chem.* **1974**, *8*, 167–174. (b) Bloomquist, D. R.; Willett, R. D. *J. Phys. Chem. Solids* **1981**, *42*, 455–460.
(22) Fletcher, R.; Hansen, J. J.; Livermore, J.; Willett, R. D. *Inorg. Chem.* **1983**, *22*, 330–334.
(23) Willett, R. D. *J. Coord. Chem.* **1988**, *19*, 253–263.
(24) Willett, R. D. *Acta Crystallogr., Sect. B* **1988**, *B44*, 503–508.
(25) Landee, C. P.; Willett, R. D. *Phys. Rev. Lett.* **1979**, *43*, 463–66. The five crystallographically inequivalent copper ions in the chain structure of TMCuC require five independent intrachain nearest-neighbor exchange constants. As in the $(ETrMA)_4Cu_5Cl_{14}$ susceptibility, the exchange constants cannot be easily distinguished from each other and an average exchange constant is refined instead.
(26) Swank, D. D.; Landee, C. P.; Willett, R. D. *Phys. Rev.* **1979**, *20*, 2154–2163.
(27) Geiser, U.; Gaura, R. M.; Willett, R. D.; West, D. X. *Inorg. Chem.* **1986**, *25*, 4203–4212.

not be surprising then that the exchange in a dimer with five-coordinate copper(II) is different from the exchange in a dimer with 4 + 1 coordination but a similar bifold angle. To this end we have calculated, using the extended Hückel method,[28] the energies ($\epsilon_1$ and $\epsilon_2$) of the molecular orbitals defined by Hay et al.[29] Molecular orbital energies were derived from the experimental atomic configurations of the dimeric species with valence atomic orbitals defined as Roothan–Hartree Fock double-$\zeta$ functions.[30] The energy difference for a third compound, *N*-methylphenethylammonium trichlorocuprate(II), henceforth $NMPHCuCl_3$, was calculated, since this compound also possesses the intermediate square-planar/trigonal-bipyramidal copper geometry.[31] A preliminary magnetic susceptibility data set on the last compound indicates that the intradimer exchange coupling is strongly ferromagnetic.[32] Calculated energy differences for the three compounds are 0.0816 eV ($(ETrMA)_4Cu_5Cl_{14}$), 0.0797 eV ($(1,4\text{-}DMP)_4Cu_5Cl_{14}$), and 0.0718 eV ($NMPHCuCl_3$) with the antisymmetric molecular orbital lower in energy in each case. The trend in the energy differences corresponds to the trend in the exchange interaction with the lower energy difference corresponding to the more ferromagnetic exchange constant. Since the calculated exchange constant depends on other factors, such as Coulomb and exchange integrals, we cannot make any predictions concerning the magnitudes of $J$; however, the trend in $J$ appears reasonable.

## Conclusions

The structures reported in this paper are two examples of an unusual class of metal halide compounds in which the metal ions are found with multiple coordination numbers or geometries. Remarkably, the three different coordination geometries in the two title compounds occur not about isolated metal ions but in a chain structure, illustrating the ease with which the copper(II) ion can assume not only different coordination geometries but different coordination numbers. As we have shown with the structures reported in this paper and cited in Table VII, the appearance of more than one coordination geometry can frequently be rationalized by an appeal to charge compensation effects.

Such an approach has also been very successful in the past in, for instance, explaining a series of structurally related $ACuCl_3$ uniform chains.[27] If A is a non-hydrogen-bonding cation, such as an alkali metal or tetramethylammonium ion, a tetragonally distorted octahedral structure is stabilized by involving all chloride ions in bridging resulting in the tribridged chain of face-sharing octahedra. If the A cation is capable of hydrogen bonding, then the hydrogen bonding provides a competing mechanism for charge removal from the chloride resulting in a chain of symmetrically bibridged square pyramids. Variation in the strength of hydrogen bonding results in a chain with a geometry intermediate between the two extremes. Thus, the idea of charge compensation can be very powerful in explaining the variation in geometry of a series of closely related structures.

We mention the above example to specifically point out the limitations of the charge compensation ideas as a predictive tool. The initial purpose of our investigation was to synthesize new members of the tribridged $ACuCl_3$ family. By the choice of a quaternary ammonium or pyridinium cation for the A ion, it was felt that formation of the bibridged $(CuCl_{2.5})_n$ chain would be avoided in favor of the tribridged $(CuCl_3)_n$ chain. As should be apparent from the structures determined in this work, our initial goal was frustrated. This in no way invalidates the idea of charge compensation, but it underscores the fact that it is only one of several factors that determine the structure. Long-range ionic forces, van der Waals repulsion, and other effects of the crystal packing will play a strong role in determining the geometry of the fluxional copper(II) coordination sphere as well as long-range geometrical arrangements of the structure. The cation in $(ETrMA)_4Cu_5Cl_{14}$, for example, differs from the tetramethylammonium cation only by a single methylene group, yet there is a large difference between the structures of the inorganic chains in $(ETrMA)_4Cu_5Cl_{14}$ and $TMACuCl_3$. Neither cation can form hydrogen bonds, so the difference in geometry and stoichiometry of the two compounds must be attributed to differences in the ill-defined "packing forces".

The magnetic model derived here for a spin-$^1/_2$ Heisenberg bowtie cluster can be a useful tool in studying the properties of low-lying electronic levels in other pentanuclear clusters. The energies derived from the model may be modified to fit a few different pentanuclear cluster configurations by judiciously fixing the appropriate exchange constants, as we have done for the linear pentamer.

It is not surprising that the five-coordinate bifolded dimer has different magnetic properties different from those of the 4 + 1 coordinate bifolded dimer. Developing a magneto-structural correlation for the five-coordinate species, though, is a much more complex problem. A magneto-structural correlation has been identified in several dimeric species containing exactly square-pyramidal copper; however, no study has been made of dimeric species containing the distorted square-pyramidal geometry. Reinen and Atanasov have described the distortion of the five-coordinate copper(II) complex from $D_{3h}$ symmetry in terms of six symmetry coordinates belonging to the $\epsilon'$ representation.[33] These might prove useful in parametrizing the magneto-structural correlation for this class of copper halide dimers. However, correlating the magnetic properties with these coordinates could involve generating a $J$ hypersurface in a seven-dimensional space: a problem that, simply from the lack of known dimers with distorted five-coordinate $CuCl_5^{3-}$, is intractable at the present time.

**Acknowledgment.** We wish to thank Dr. Chris Landee and Dr. John E. Drumheller in whose laboratories the magnetic susceptibility data of $(1,4\text{-}DMP)_4Cu_5Cl_{14}$ (C.L.) and $(ETrMA)_4Cu_5Cl_{14}$ (J.E.D.) were taken. We gratefully acknowledge the financial support of The Boeing Co. and the National Science Foundation (Grant CHE-8408407) in purchasing the X-ray diffractometers. This work was supported by the National Science Foundation (Grant DMR 88-03382).

**Supplementary Material Available:** Listings of organic cation bond lengths and angles, anisotropic temperature factors, hydrogen atom coordinates and temperature factors, and data collection and structure refinement conditions and parameters (7 pages); tables of calculated and observed structure factors (51 pages). Ordering information is given on any current masthead page.

(28) Hoffmann, R. *J. Chem. Phys.* **1963**, *39*, 1397–1412.
(29) Hay, P. J.; Thibeault, J. C.; Hoffmann, R. *J. Am. Chem. Soc.* **1975**, *97*, 4884–4899.
(30) Clementi, E.; Rosetti, C. *At. Nucl. Data Tables* **1974**, *14*, 177–478.
(31) Harlow, R. L.; Wells, W. J., III; Watt, G. W.; Simonsen, S. H. *Inorg. Chem.* **1974**, *13*, 2860–2864.
(32) Willett, R. D. Unpublished work.
(33) Reinen, D.; Atanasov, M. *Chem. Phys.* **1989**, *136*, 27–46.